Academic Journal of Science and Technology
ISSN: 2771-3032 | Vol. 10, No. 1, 2024

Observation of Multiple Topological edge States in Square-Root electric circuits

Jingxiang Gao*, Ming Zhang, Xiefei Cheng, Xingcheng Tang, Runjia Guo

School of Physics and Optoelectronic Engineering, Guangdong University of Technology, Guangzhou 510006, China
* Corresponding author

Abstract: Square-root topological states are new topological phases, whose intriguing topological properties are inherited from the parent lattice Hamiltonian. Because of the square-root procedure, the bulk gap of the parent Hamiltonian is doubled. In this letter, we report the observation of the square-root topological insulators (SRTIs) in topological LC circuits, whose squared Hamiltonian includes a Su-Schrieffer-Heeger (SSH) model, a well-known example of topological insulators (TI). The multiple localized edge states falling in different bandgaps are observed with characteristic phase structures, in sharp contrast to the discrete diffraction in a topologically trivial structure. These edge states with zero energy are manifested by a prominent impedance peak at the midgap frequency and directly observed by impedance measurements. Our work opens up an alternative gateway towards actively controllable topological systems and may bring about new possibilities in topology-driven electronic devices.

Keywords: Topological insulator, square-root operation, edge states, electrical circuit.

1. Introduction

Topological band theory provides a theoretical framework for the abundance of topological states of quantum matter, such as insulators[1,2], (semi-)metals[3], and superconductors[4,5]. The system described by Hamiltonians has been the main focus of research on topological band theory. This theory can be used to classify the structures of periodic energy bands by using topological invariants related to the eigenstates of energy in the momentum space. In the past few years, the intriguing topological physical effects have been extended to artificial periodic structures including photonic crystals[6-9], phononic crystals (PCs)[10-16], electric circuits[13,17-19], etc. Due to the high precision of sample fabrication, the electric circuit system provides an excellent platform to explore intriguing topological properties. To date, searching and realizing new topological states in circuits continues to attract a great deal of attention[20-31].

Recently, a square-root TI (SRTI) is proposed[32]. Its topological properties are demonstrated to be inherited from the parent Hamiltonian [33-36]. The square-root procedure had played an important role in deriving the Dirac equation in relativistic quantum mechanics from the quadratic Klein-Gordon equation, which revealed the chirality for electrons. This procedure provides an antidiagonal block matrix form and leads to symmetric spectra for square-root Hamiltonian [37-40]. For lattice models, SRTI can be generated by inserting additional sites and breaking up the coupling between the original sites. So far, only few experiments for SRTI have been realized in quantum matter. Very recently, electric circuit experiment confirmed the square-root topological insulator[33,41,42]. In order to directly observe the finite-energy topological states, scientists introduced the extra grounded inductors to each node, which shifts topological states to zero-energy without affecting their spatial distributions. So obtaining "nonzero-energy" topological modes with zero energy is the point in all kinds of square-root electric circuits.

In this letter, we demonstrate the multiple topological edge States in square-root electric circuits, by inserting a set of additional nodes in the LC SSH model. Because of the square-root procedure, the bulk gap of the parent Hamiltonian is doubled. We find that the multiple localized edge states fall in different bandgaps with characteristic phase structures. These edge states with zero energy are directly observed by impedance measurements. Our work substantiates the emerging square-root TI and may bring about new possibilities in actively controllable topology-driven electronic devices.

2. Results and Discussion

Su-Schrieffer-Heeger Electrical Circuit.

We start with the non-Hermitian SSH chain, which is shown in the upper panel of Figure 1a. The SSH chain consists of two nonequivalent sites (A and B) in each unit cell. The intracell and intercell coupling strengths are denoted as ν^2 and μ^2. Following the general recipe for the construction of SRTI developed by Ezawa,[43] by inserting another two sites (C and D) which separate the original ones and taking the square root of coupling strengths, as shown in the lower panel of Figure 1a, the square-root SSH chain has been designed. Now, there are four sites labeled by A, B, C, and D in each unit cell, with symmetrical intracell coupling ν, symmetrical intracell coupling μ and symmetrical intercell coupling μ. According to Kirchhoff's law and Ohm's law, we can formulate the current and voltage equations for the 11 nodes. After simplification of the resulting current equation, we obtained the following:

$$I_{1-4} = i\omega[\left(C_1 + C_2 + C_3 - \frac{1}{\omega^2 L}\right) I + H(k)]V_{1-4} \quad (1)$$

with

$$H(k)^2 = \begin{bmatrix} 0 & 0 & C_1 & C_2 e^{-ik} \\ 0 & 0 & C_1 & C_2 \\ C_1 & C_1 & 0 & 0 \\ C_2 e^{ik} & C_2 & 0 & 0 \end{bmatrix}^2 = \begin{bmatrix} H_{par} & 0_{2\times2} \\ 0_{2\times2} & H_{res} \end{bmatrix} \quad (2)$$

with matrix elements $H_{par} = (C_1^2 + C_2^2)I_{2\times2} + H_{org}$ with

$$H_{org} = \begin{bmatrix} 0 & C_1^2 + C_2^2 e^{-ik} \\ C_1^2 + C_2^2 e^{ik} & 0 \end{bmatrix} \quad (3)$$

Where I represents the 4 × 4 unit matrix, $I_{1-4}$and V_{1-4} denote the input currents and response voltages of four nodes, respectively. The residual Hamiltonian, denoted as H_{res}, consistently represents a topologically mundane system, while H_{par} stands for the Hamiltonian of the SSH chain. The square of $H(k)$ equals the direct sum of the parent Hamiltonian H_{par} and a residual Hamiltonian H_{res}. As $H(k)$ corresponds to the square-root of H_{par}, we refer to this new composite lattice model as the square-root SSH chain.

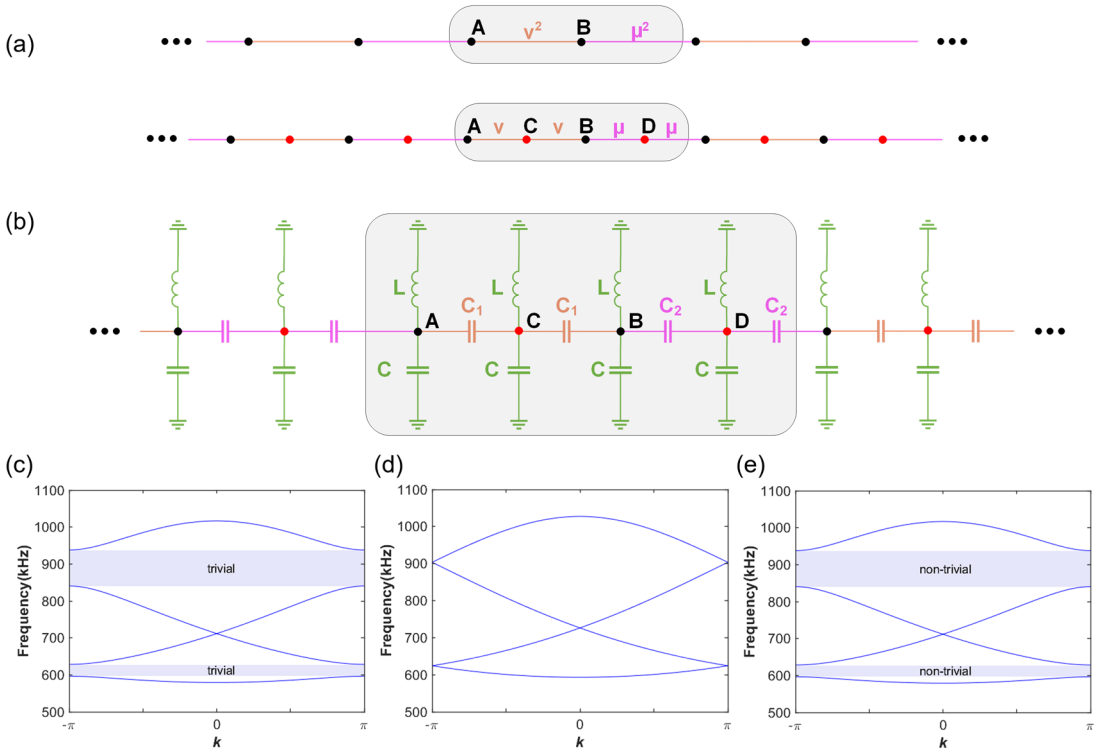

Figure 1. Lattice models for SRTIs. (a) Top panel: the schematic for the SSH model with squared hopping parameters. Bottom panel: the schematic for the square-root SSH model with intracell coupling ν and intercell coupling μ. (b) Circuit implementation of the square-root SSH model, and the gray solid box marks one unit cell. (c)–(e) Band structure for different parameter: $C_1 = 1.5$ nF, $C_2 = 1$ nF for (c), $C_1 = C_2 = 1$ nF for (d), $C_1 = 1$ nF, $C_2 = 1.5$ nF for (e). The parameters are set to $L = 10$ μH.

When analyzing the eigenvalues of the circuit system, assuming $I_{1-4} = 0$, Eq. (1) can be reformulated as $H(k)V = (C_1 + C_2 - \frac{1}{\omega^2 L})V$. By solving for the eigenvalue ε_n of $H(k)$, we ultimately derive the dispersion relation of the circuit as $f = 1/2\pi\sqrt{2C_1 + 2C_2 + \varepsilon_n}$. It is important to note that we mitigate the impact of the main diagonal elements on the system during resonance by judiciously selecting $C_a = C_1 + C_2$, $C_b = 2C_2$ and $C_c = 2C_1$.

The band structures for different capacitance coupling are shown in Figure 1c-e, which is gapped at $k = \pm\pi$ point for $C_1/C_2 \neq 1$. It is therefore possible to realize the topological insulator phase due to the gap opening. The band structures in Figure 1c and Figure 1e show the same gap opening conditions. However, we suggest that there is a non-trivial bandgap in the former case, while the latter was trivial. In Figure 1d, when $C_1 = C_2$ the bandgap closes at $k = \pm\pi$, representing topological phase transition points.

For each band, we can evaluate a 1D topological invariant, Zak's winding phase $\theta_i = \int_{BZ} dk A_i(k)$, where $A_i(k) = i\langle v_i(k)|\partial_k|v_i(k)\rangle$ is the Berry connection of the ith band and $|v_i(k)\rangle$ is the corresponding eigenstate[44]. For a standard 1D topological insulator, the winding phase takes quantized values of π (or 0) corresponding to encircling (or not encircling) a singularity in quasi-momentum phase space. When $C_1 = 1$ nF, $C_2 = 1.5$ nF, there are four bands with the quantized Zak's winding phases ($\theta = -\pi/2$).

Edge States.

We consider a finite-size SSH chains circuit with $N = 40$ nodes. The Laplacian of the circuit can be written as

$$J(\omega) = \begin{bmatrix} M & 0 & -J_1 & 0 & 0 & \cdots \\ 0 & M & -J_1 & -J_2 & 0 & \cdots \\ -J_1 & -J_1 & M & 0 & 0 & \cdots \\ 0 & -J_2 & 0 & M & -J_2 & \cdots \\ 0 & 0 & 0 & -J_2 & M & \cdots \\ \vdots & \vdots & \vdots & \vdots & \vdots & \ddots \end{bmatrix}_{N \times N} \quad (4)$$

with $M = i\omega(2C_1 + 2C_2 - 1/\omega^2 L)$ and $J_m = i\omega C_m$ $(m = 1,2)$.

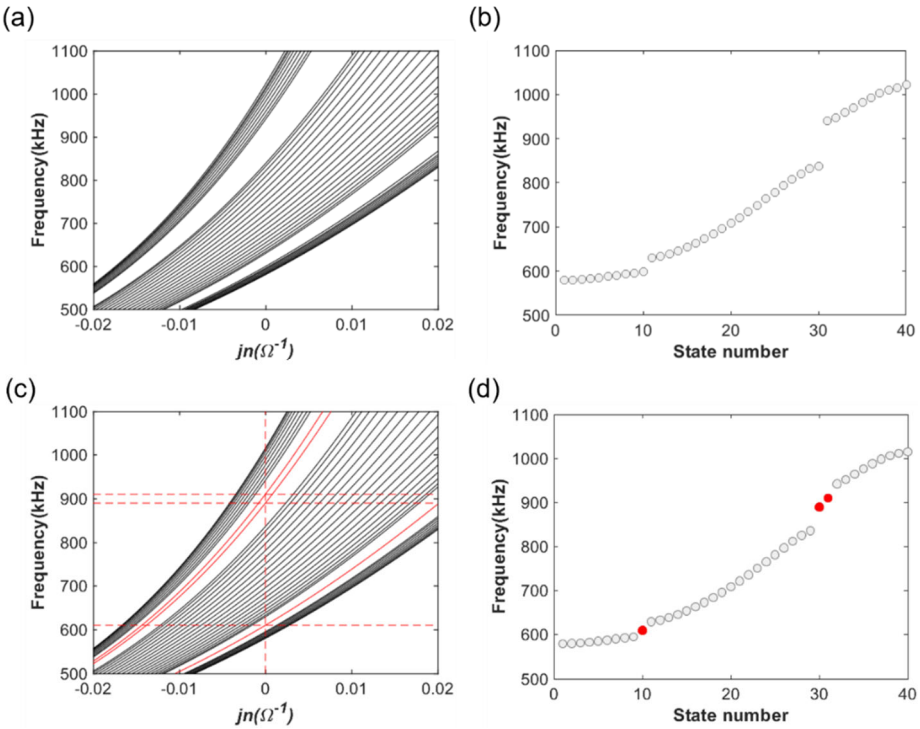

Figure 2. The admittance spectrums and eigenfrequencies spectrums of the circuit model. (a), (b) The admittance spectrums and eigenfrequencies spectrums of circuit model for $C_1/C_2 = 3/2$. (c)The theoretical spectrum of J(ω) depending on the frequency with grounded inductors L, where the red segments denote the edge states. (d) Admittances for $C_1/C_2 = 2/3$ with $L = 10$ μH. The red and gray dots represent the edge and bulk, respectively.

Subsequently, we computed the eigenfrequencies and eigenfunctions of $J(\omega)$. Figures 2a and 2b display the admittance spectrum eigenfrequencies spectrum of the square-root SSH chain when $C_1/C_2 = 3/2$. It can be observed that there are no isolated states, indicating that the system is trivial in this case. Figure 2c displays the admittance spectrum of the square-root SSH chain, wherein the edge states are plotted as red curves. Figure. 2d shows the eigenvalue spectrum and edge states in the bandgap, where red circles and grey circles represent edge states and bulk states, respectively. The three edge degenerate states are numerically identified at three frequencies, $f_{01} = 610$ kHz, $f_{02} = 890$ kHz and $f_{03} = 910$ kHz ,with their density distributions localized at the left and right end of the model. In the theoretical calculations, we adopt $L = 10$ μH.

The nontrivial topological feature of the 1D topological insulator is manifested by its distinct edge state, which appears at the boundaries of a finite chain. However, it should be noted that the observables of topological circuits are different from those in the quantum and photonics systems. Topological circuits are commonly studied through a two-point impedance measured between two adjacent nodes, a and b, subject to an external current excitation, I_0, flowing through them, which is expressed as[24,45,46]

$$Z_{ab} = \frac{V_a - V_b}{I_0} = \sum_n \frac{|\psi_{n,a} - \psi_{n,b}|^2}{j_n}, \quad (5)$$

in which $\psi_{n,i}(i = a\ or\ b)$ and $j_n(\omega)$ represent the eigenstates and eigenvalues of $J(\omega)$, respectively. As the root of $j_n(\omega)$ corresponds to the eigenfrequency of the circuit, $Z_{ab}(\omega)$ diverges when the denominator $j_n(\omega)$ crosses zero. Consequently, each pole in $Z_{ab}(\omega)$ signifies a mode (block or edge) in a finite circuit. Therefore, strong resonant peaks on the ω_0 impedance spectra can be used to identify topological states at circuit boundaries.

Impedance observation.

We choose electric elements $C_1 = 1$ nF, $C_2 = 1.5$ nF, $L = 10$ μH. Figure 3a shows tight-binding model of ten unit cells. We determine the ground impedance between two representative nodes and other bulk nodes as a function of excitation frequency, as shown in Figure 3b, where we select the A, B, and other bulk nodes to characterize the properties of the edge and bulk states, respectively. In the theoretical calculation, we have averaged the result after 10^3 realizations of uniformly distributed disorder (we assume a 2% tolerance of each electric element). At the resonant frequency f_{01}, f_{02} and f_{03}, theoretical curves(red) display a strong peak, which confirms the very existence of the edge states. We demonstrate the distribution of the theoretical impedance in this circuit (see Figure 3c-e).

Robustness of the edge states.

Topological states show resilience and robustness against disorder and defects in general. In order to examine the robustness of the BIC, we introduce defects in the fourth and seventh unit cells of the circuit structure. The specific circuit diagrams are shown in Figure 4a. Figure 4b and Figure 4c depict the impedance map at node A and B, the impedance at the frequency f_{01}, f_{02} and f_{03} still shows the strong localization around the original edge. The frequency of the edge states remains stable.

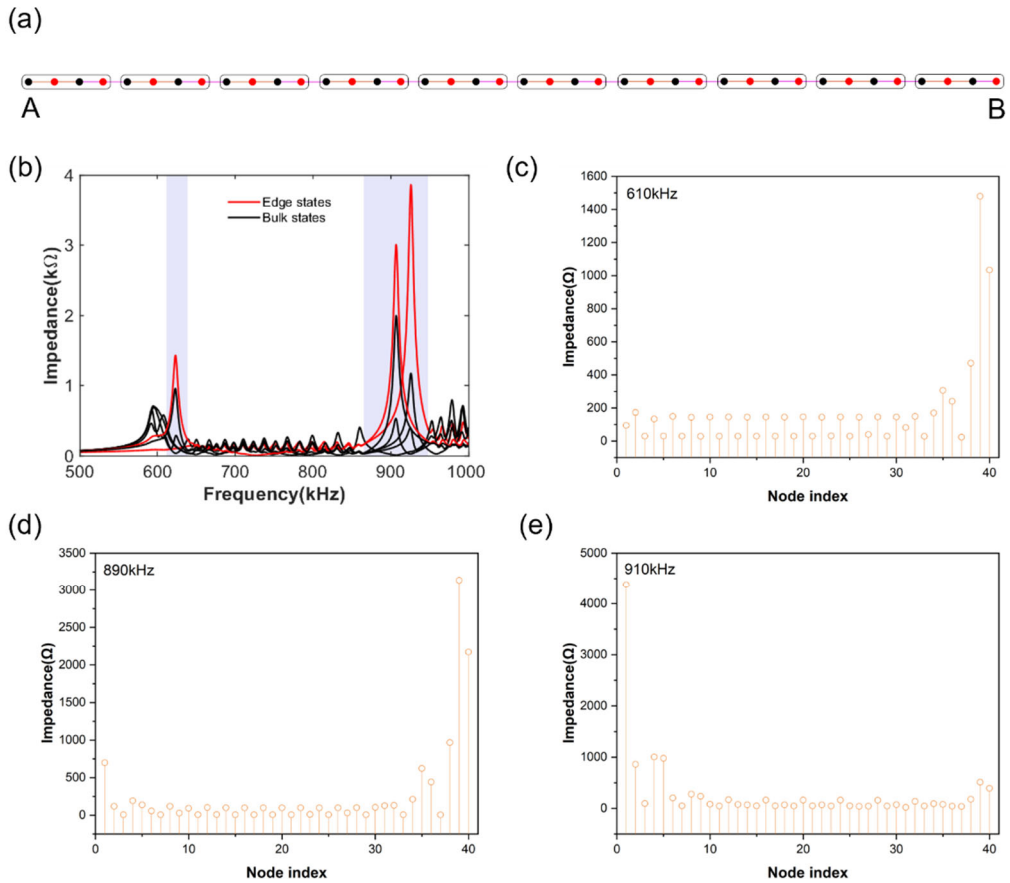

Figure 3. Realization of the SRTI in LC circuit. (a) Tight-binding model of ten unit cells. (b) Theoretical (frequency domain solver) impedance spectra of the finite circuit chain. (c)-(e) Distribution of the measured impedance for the edge states at f_{01}, f_{02} and f_{03}, respectively.

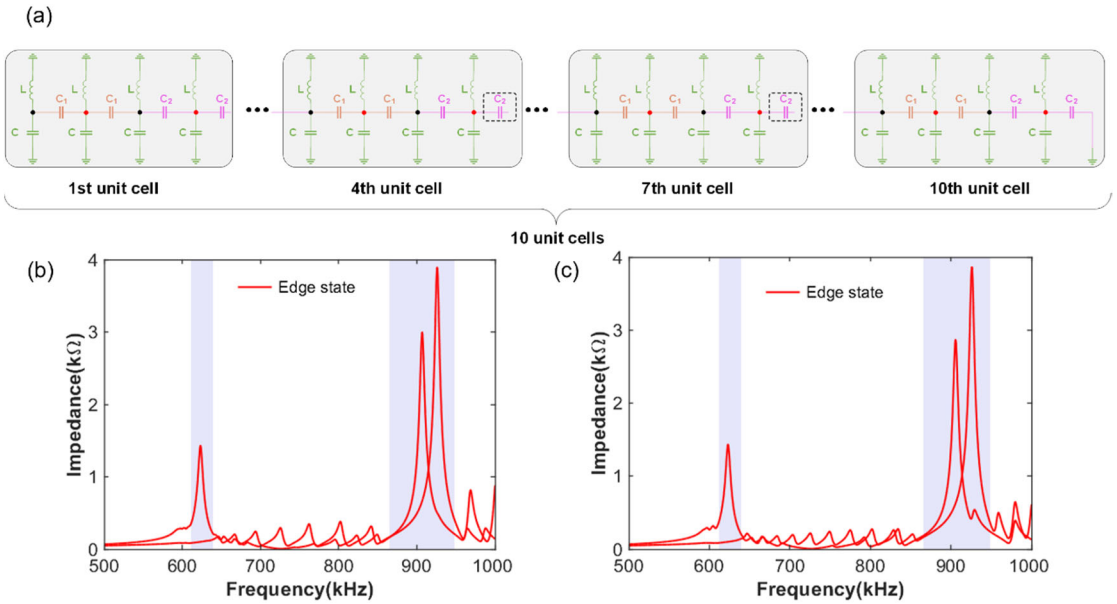

Figure 4. Robustness verification of the square-root LC circuit. (a) Circuit diagrams of the defects introduced in the fourth and seventh unit cells, respectively. (b) (c) Impedance simulation diagrams at points A and B.

3. Conclusion

In summary, we presented observation of the square-root topological insulators in LC circuits. Here, a set of additional inductors and capacitors are inserted in the identical LC SSH model. Three edge states are observed in two different band gaps with different phase structures. The robustness of the edge states against different defects is also demonstrated. Our work not only provides a new platform to substantiate the emerging square-root TI, but also offers possible applications for advanced electronic devices such as multifrequency sensing or multiband filter.

References

[1] D. J. Thouless, M. Kohmoto, M. P. Nightingale, and M. den Nijs, Physical Review Letters 49 (6), 405 (1982).

[2] C. L. Kane and E. J. Mele, Physical Review Letters 95 (14), 146802 (2005).

[3] Mustafa Sarısaman and Murat Tas, Journal of Applied Physics 126 (16), 163102 (2019).

[4] Ling Lu, Liang Fu, John D. Joannopoulos, and Marin Soljačić, Nature Photonics 7 (4), 294 (2013).

[5] Shuifang Lu, Xin Zhang, Fugen Wu, Yuanwei Yao, and Zongwang Chen, Journal of Applied Physics 120 (4), 045102 (2016).

[6] N. Prodanović, V. Milanović, and J. Radovanović, Journal of Physics A: Mathematical and Theoretical 42 (41), 415304 (2009).

[7] Wonjoo Suh, Olav Solgaard, and Shanhui Fan, Journal of Applied Physics 98 (3), 033102 (2005).

[8] Wonjoo Suh, M. F. Yanik, Olav Solgaard, and Shanhui Fan, Applied Physics Letters 82 (13), 1999 (2003).

[9] Bo Zhen, Chia Wei Hsu, Ling Lu, A. Douglas Stone, and Marin Soljačić, Physical Review Letters 113 (25), 257401 (2014).

[10] Kun Ding, Guancong Ma, Meng Xiao, Z. Q Zhang, and C. T Chan, Physical Review X 6 (2), 021007 (2016).

[11] Stefan Hein, Werner Koch, and Lothar Nannen, Journal of Fluid Mechanics 692, 257 (2012).

[12] A. A Lyapina, D. N Maksimov, A. S Pilipchuk, and A. F Sadreev, Journal of Fluid Mechanics 780, 370 (2015).

[13] Yi-Xin Xiao, Guancong Ma, Zhao-Qing Zhang, and C. T Chan, Physical Review Letters 118 (16), 166803 (2017).

[14] Jin Li, ChengXin Deng, Kun Zhang, Qiao Lu, and Hai Yang, Applied Physics Letters 123 (25), 253101 (2023).

[15] Luohong Liu, Tianzi Li, Qicheng Zhang, Meng Xiao, and Chunyin Qiu, Physical Review Letters 130 (10), 106301 (2023).

[16] Qicheng Zhang, Daehun Lee, Lu Zheng, Xuejian Ma, Shawn I. Meyer, Li He, Han Ye, Ze Gong, Bo Zhen, Keji Lai, and A. T. Charlie Johnson, Nature Electronics 5 (3), 157 (2022).

[17] J. J. Tang, F. Y. Ma, F. Li, H. L. Guo, and D. Zhou, FRONTIERS OF PHYSICS 18 (3) (2023).

[18] You Wang, Hannah M. Price, Baile Zhang, and Y. D. Chong, Nature Communications 11 (1), 2356 (2020).

[19] Jien Wu, Xueqin Huang, Yating Yang, Weiyin Deng, Jiuyang Lu, Wenji Deng, and Zhengyou Liu, Physical Review B 105 (19), 195127 (2022).

[20] Victor V. Albert, Leonid I. Glazman, and Liang Jiang, Physical Review Letters 114 (17), 173902 (2015).

[21] Motohiko Ezawa, Physical Review B 98 (20), 201402 (2018).

[22] Tal Goren, Kirill Plekhanov, Félicien Appas, and Karyn Le Hur, Physical Review B 97 (4), 041106 (2018).

[23] Yakir Hadad, Jason C. Soric, Alexander B. Khanikaev, and Andrea Alù, Nature Electronics 1 (3), 178 (2018).

[24] Stefan Imhof, Christian Berger, Florian Bayer, Johannes Brehm, Laurens W. Molenkamp, Tobias Kiessling, Frank Schindler, Ching Hua Lee, Martin Greiter, Titus Neupert, and Ronny Thomale, Nature Physics 14 (9), 925 (2018).

[25] Ching Hua Lee, Stefan Imhof, Christian Berger, Florian Bayer, Johannes Brehm, Laurens W. Molenkamp, Tobias Kiessling, and Ronny Thomale, Communications Physics 1 (1), 39 (2018).

[26] B. Liu, Y. Li, B. Yang, X. P. Shen, Y. T. Yang, Z. H. Hang, and M. Ezawa, PHYSICAL REVIEW RESEARCH 5 (4) (2023).

[27] Shuo Liu, Wenlong Gao, Qian Zhang, Shaojie Ma, Lei Zhang, Changxu Liu, Yuan Jiang Xiang, Tie Jun Cui, and Shuang Zhang, Research 2019.

[28] Yuehui Lu, Ningyuan Jia, Lin Su, Clai Owens, Gediminas Juzeliūnas, David I. Schuster, and Jonathan Simon, Physical Review B 99 (2), 020302 (2019).

[29] Kaifa Luo, Rui Yu, and Hongming Weng, Research 2018.

[30] Jia Ningyuan, Clai Owens, Ariel Sommer, David Schuster, and Jonathan Simon, Physical Review X 5 (2), 021031 (2015).

[31] Erhai Zhao, Annals of Physics 399, 289 (2018).

[32] J. Arkinstall, M. H. Teimourpour, L. Feng, R. El-Ganainy, and H. Schomerus, Physical Review B 95 (16), 165109 (2017).

[33] Lingling Song, Huanhuan Yang, Yunshan Cao, and Peng Yan, Nano Letters 20 (10), 7566 (2020).

[34] Lingling Song, Huanhuan Yang, Yunshan Cao, and Peng Yan, Nature Communications 13 (1), 5601 (2022).

[35] Wenchao Yan, Daohong Song, Shiqi Xia, Junfang Xie, Liqin Tang, Jingjun Xu, and Zhigang Chen, ACS Photonics 8 (11), 3308 (2021).

[36] Huanhuan Yang, Z. X. Li, Yuanyuan Liu, Yunshan Cao, and Peng Yan, Physical Review Research 2 (2), 022028 (2020).

[37] Z. G. Geng, Y. G. Peng, H. Z. Lv, Z. Xiong, Z. J. Chen, and X. F. Zhu, JOURNAL OF PHYSICS-CONDENSED MATTER 34 (10) (2022).

[38] S. Q. Guo, G. W. Pan, J. K. Huang, R. M. Huang, F. J. Zhuang, S. J. Su, Z. L. Lin, W. B. Qiu, and Q. Kan, APPLIED PHYSICS LETTERS 123 (4) (2023).

[39] M. Yan, X. Q. Huang, L. Luo, J. Y. Lu, W. Y. Deng, and Z. Y. Liu, PHYSICAL REVIEW B 102 (18) (2020).

[40] W. C. Yan, W. Z. Cheng, W. J. Liu, Q. C. Liu, and F. Chen, OPTICS LETTERS 48 (14), 3765 (2023).

[41] Ruo-Long Zhang, Qing-Ping Wu, Mei-Rong Liu, Xian-Bo Xiao, and Zheng-Fang Liu, Annalen der Physik 534 (6), 2100497 (2022).

[42] Shengqun Guo, Guangwu Pan, Jinke Huang, Ruimin Huang, Fengjiang Zhuang, Shaojian Su, Zhili Lin, Weibin Qiu, and Qiang Kan, Applied Physics Letters 123 (2023).

[43] Motohiko Ezawa, Physical Review Research 2 (3), 033397 (2020).

[44] J. Zak, Physical Review Letters 62 (23), 2747 (1989).

[45] Ling Lin, Yongguan Ke, and Chaohong Lee, Physical Review B 103 (22), 224208 (2021).

[46] Shuo Liu, Shaojie Ma, Cheng Yang, Lei Zhang, Wenlong Gao, Yuan Jiang Xiang, Tie Jun Cui, and Shuang Zhang, Physical Review Applied 13 (1), 014047 (2020).